ACS Photonics

pubs.acs.org/journal/apchd5 Article

Quasinormal Coupled-Mode Analysis of Dynamic Gain in Exceptional-Point Lasers

Hao He,* Xingwei Gao, Alexander Cerjan,* and Chia Wei Hsu

Cite This: *ACS Photonics* 2025, 12, 4150−4160 Read Online

ACCESS | Metrics & More | Article Recommendations | Supporting Information

ABSTRACT: One of the key features of lasers operating near exceptional points (EPs) is that the gain medium can support an oscillating population inversion above a pump threshold, leading to self-modulated laser dynamics. This unusual behavior opens up new possibilities for frequency comb generation and temporal modulation. However, the dynamic population inversion couples signals with different frequencies and is difficult to capture using conventional temporal coupled-mode theory (TCMT) based on stationary saturable gain. In this paper, we develop a perturbative coupled-mode analysis framework to capture the spatial-temporal dynamics of near-EP lasers. By decomposing discrete frequency generation into multiple excitations of resonant modes, our analysis establishes a minimal physical model that translates the local distribution of dynamic population-inversion into a resonant modal interpretation of laser gain. This work enables the exploration of unique properties in this self-time-modulated systems, such as time-varying scattering and nonreciprocal transmission.

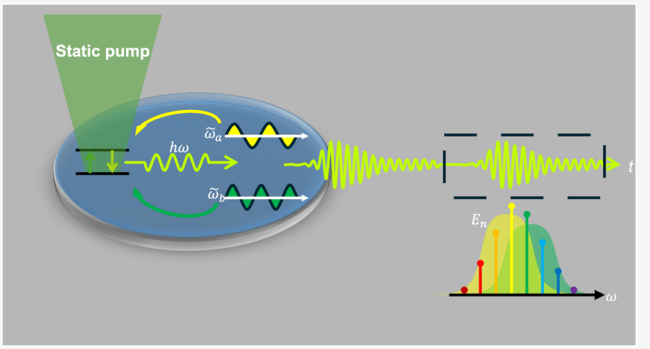

KEYWORDS: *non-Hermitian, photonics, laser theory, frequency comb, quasinormal mode, coupled-mode analysis*

1. INTRODUCTION

Non-Hermiticity is a crucial feature of optical systems due to the ubiquity of both material absorption and radiative losses to the surrounding environment.[1] Among various non-Hermitian effects, exceptional points (EP)—spectral singularities in non-Hermitian systems—are crucial to understand because they fundamentally alter a system's response and promote a variety of optical applications, such as enhanced sensitivity and chiral control of light.[2−11] Lasers have been an ideal platform to demonstrate key characteristics of EPs as they exhibit a natural way to implement spatially nonuniform gain and loss, as is required for EP formation.[12−16] Recent studies found that the interplay between EPs and lasers reveals exciting opportunities to control laser dynamics, such as loss-induced lasing,[17] reverse pump dependence,[15,18] and robust single-mode operation.[19,20] Generally, only one mode among the paired resonances of an EP lases at a single time and so the carrier populations of the gain medium can be approximated as stationary. In these cases, the other latent resonances(s) of an EP can lead to undesired laser line width broadening while maintaining single mode operation.[21−23]

However, if a laser is driven sufficiently close to an EP, the static gain approximation is expected to fail.[24−26] In this near-EP regime, the time-scale of any relaxation oscillations due to spontaneous emission can be sufficiently long-lived that these spontaneous emission events, subsequently amplified, completely destabilize the system's single mode operation. In such a case, even though no other cavity resonance reaches its lasing threshold, the system will still spontaneously evolve into a frequency comb with dynamic carrier populations. Heuristically, the beat notes generated by oscillating inversion interacting with the lasing mode destabilizes the stationary laser gain and induces coherent oscillations of the nonresonant population inversion inside the gain medium, a process that is enhanced by the spatial coalescence of two modal profiles guaranteed by their proximity to the EP, and generating a cascade of new frequencies resulting in a self-generating frequency comb. However, the appearance of a self-generated frequency comb presents a problem for modeling such systems because the combined spatial-temporal complexity involves nonlinear interactions across two different time scales. Typical laser models (Figure 1) such as the steady-state *ab initio* laser theory (SALT) and the rate equation description fail to model the dynamic gain near EP or do not yield analytic prediction for the comb's behavior,[26−30] because they either rely on the assumption of static population inversion (SALT) or over-simplify the geometry that is crucial for achieving the EP-

Received: January 9, 2025
Revised: July 16, 2025
Accepted: July 17, 2025
Published: July 29, 2025

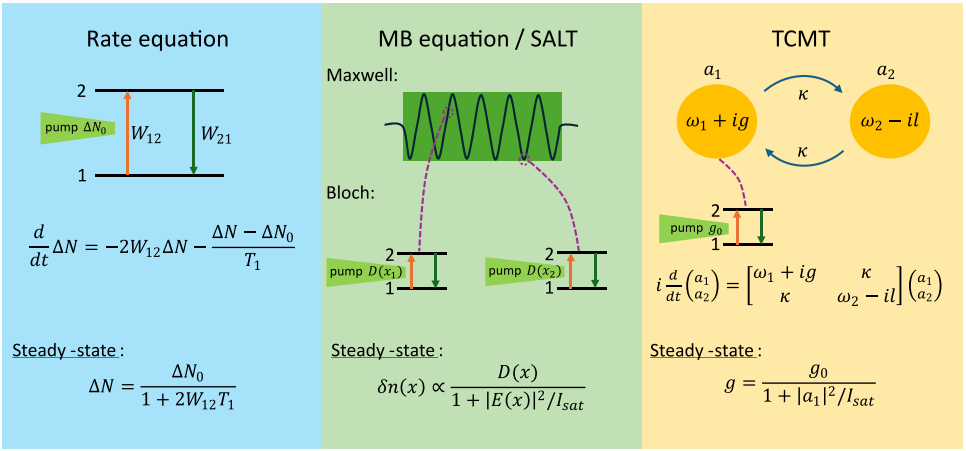

Figure 1. Schematic of typical laser models. The rate equation phenomenologically describes the light-matter interaction in time while ignoring the geometry of laser cavity.[38] W_{12} and W_{21} are the upward and downward stimulated-transition probabilities and $W_{12} \equiv W_{21}$. $\Delta N = N_2 - N_1$ is the population inversion and ΔN_0 is the pumped thermal-equilibrium population inversion without external electric field. The Maxwell-Bloch equations couple electric field with local two-level atoms, and reduce to a nonuniform perturbation on the refractive index $\delta n(x)$ caused by spatial hole burning in the static-inversion regime.[28] Typical TCMT uses a simple saturable gain g to model the complex laser dynamics.[6]

condition (rate equation approach). There have been attempts combining TCMT formalism with rate equation description of the carrier dynamics to model typical laser characteristics,[25,31−36] but only few of them fully accounts for the spatiotemporal dependence of the population inversion. As the spatial distribution of population inversion is subject to saturation and thus nonuniform in space, ignoring the saturation in space-dependent population inversion only predicts linear and near threshold or incomplete saturable lasing features.[25,31−35] The temporal nonstationary population inversion also excludes the existing TCMT framework for static saturable absorption as the gain medium manifest dynamic carriers behavior.[36] The only previously proven approach to fully account for such dynamic gain is via brute-force finite-difference time-domain (FDTD) simulations of the Maxwell-Bloch (MB) equations across the entire laser cavity,[24] which requires unusually high numerical precision due to the high sensitivity of EP phenomena to numerical error. Due to such unusually high numerical precision needed for discretizing this near-EP system, the rigorous TCMT approach capable of handling full spatialtemporal dependence of the population inversion would encounter great numerical challenge and thus become unscalable for realistic near-EP laser cavity design.[37] Although the periodic-inversion *ab initio* laser theory (PALT) analysis on MB equations provides a quantitative method for numerical computation,[24] it does not yield an intuitive model to explain how frequency combs are generated via local laser nonlinearities.

Here, we develop a rigorous coupled-mode analysis of the laser gain by bridging the local distribution of population inversion with the resonant modal interaction near an EP. In doing so, we also demonstrate that the spatial nonuniformity induced by hole-burning in both the single-mode laser and the EP-laser can be accurately treated using a Padé approximant. The response of the passive cavity to the pump-induced polarization is decomposed into discrete excitations of the passive resonant modes, which is known as a quasinormal mode (QNM) expansion.[39−43] The quasinormal coupled-mode description for such EP-lasers, that we will refer to as QNM-PALT, can be expressed as integral equations with only the expansion coefficients and lasing frequencies as unknowns. These integral equations establish the connection from local distribution of population inversion to the cavity modal interaction and quantitatively describe the enhancement of the spatial overlap between the two EP-modes with the dynamic gain. Under the weak spatial coupling limit, which is automatically satisfied due to the EP-laser condition,[24] combined with the Padé approximant of the integral function, QNM-PALT can be expressed as a purely algebraic problem of the expansion coefficients without spatial dependence. Compared with other frameworks for modeling lasers, QNM-PALT inherits both the rigor of the MB equations and conciseness of temporal coupled-mode theory (TCMT) analyses, while overcoming the difficulties stemming from dynamic gain in standard phenomenological TCMT approaches that assume static laser gain.[6,44−46] This simple physical model combined with its computational efficiency enables further exploration of EP lasers, including novel laser properties due to the self-time-modulation and optimization for compact source of coherent frequency combs. The dynamic gain modeled by this QNM-PALT framework also opens new opportunities for introducing time modulation to optical systems,[47−50] for instance, the bistability and cascade of period-doubling have been found to exist in such system.[51] Moreover, the Padé approximant we adopt here provides an efficient series expansion technique to simplify the saturable laser nonlinearity and is expected to simplify the description of gain competition in multimode lasers.[28]

The remainder of this paper is organized as follows: In Section 2, we provide the theoretical background of QNM and the corresponding QNM expansion equations. In Section 3, we apply the QNM expansion formalism to the single-mode lasing in a 1D system and introduce the Padé approximant, a series expansion to simplify the field expansion integral. In Section 4, we apply the QNM expansion method to the general frequency comb solution in a 1D multilayer near-EP laser system. In Section 5, we apply the developed framework to a 2D near-EP coupled-disk laser system. We conclude in Section 6.

https://doi.org/10.1021/acsphotonics.5c00086
ACS Photonics 2025, 12, 4150−4160

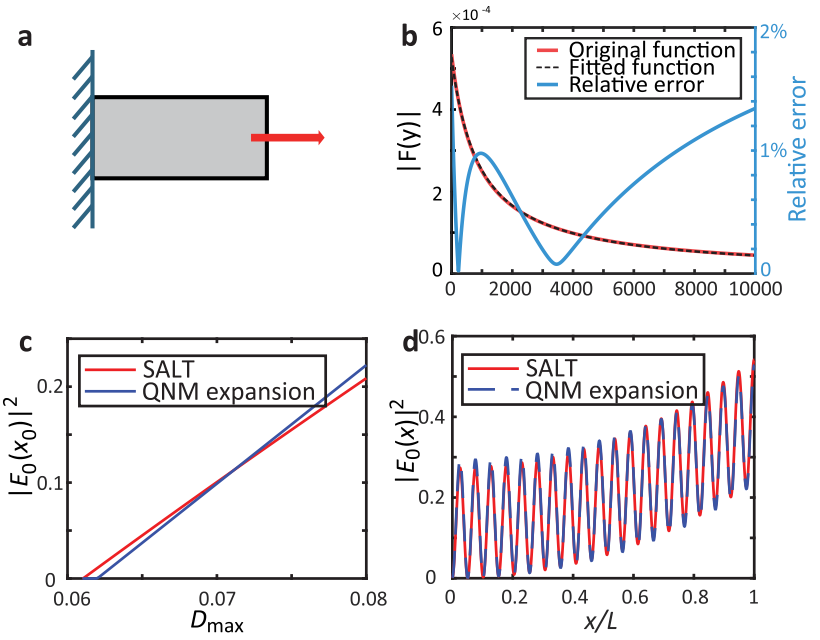

Figure 2. Validating the Padé approximation using a single-mode laser in 1D cavity. (a) The cavity is bounded on one side by a perfect mirror and open to free space on the other side. The refractive index of the medium is $n = 1.5$ and the length of the lasing medium is L. Parameters of two-level atoms are $\omega_{ab} = 40c/L$ and $\gamma_\perp = 4c/L$. The pump profile here is chosen uniform inside the laser cavity. (b) Comparison of the original integral function and its Padé approximant. Padé approximant provides an accurate approximation as the relative error lies within 2%. (c) The relation between the field intensity at certain point $x = x_0 = 0.24L$ away from the left mirror inside the laser cavity and the pumping strength D_{max} computed from SALT and QNM expansion, respectively. (d) The intensity distribution across the laser cavity at $D_{max} = 0.08$ from SALT and QNM expansion, respectively.

2. THEORETICAL BACKGROUND—QUASINORMAL MODES AND QUASINORMAL MODE EXPANSION

QNMs are the eigenmodes of non-Hermitian open systems. In a nondispersive passive system consisting of resonators that may be absorbing and are surrounded by free space, the QNMs can be defined in terms of the vectorial electomagnetic field $[\tilde{\boldsymbol{E}}(\boldsymbol{r}), \tilde{\boldsymbol{H}}(\boldsymbol{r})]$. Specifically, the nth QNM is defined as the solution of the source-free wave equation,

$$\nabla \times \tilde{\boldsymbol{E}}_n(\boldsymbol{r}) = i\tilde{\omega}_n \boldsymbol{\mu}(\boldsymbol{r})\tilde{\boldsymbol{H}}_n(\boldsymbol{r}) \tag{1}$$

$$\nabla \times \tilde{\boldsymbol{H}}_n(\boldsymbol{r}) = -i\tilde{\omega}_n \boldsymbol{\varepsilon}(\boldsymbol{r})\tilde{\boldsymbol{E}}_n(\boldsymbol{r}) \tag{2}$$

with outgoing boundary conditions.[39,52,53] Here, $\boldsymbol{\varepsilon}(\boldsymbol{r})$ and $\boldsymbol{\mu}(\boldsymbol{r})$ are the permittivity and permeability of the passive resonator system, which are generally complex to account for possible material absorption. The eigenvalue $\tilde{\omega}_n = \omega_n - i\gamma_n$ is the nth QNM frequency and is also complex. Due to the causality constraint that analyticity should be maintained in the upper half plane of complex frequency,[54] all QNM eigen-frequencies should have a negative imaginary part, i.e., $\gamma_n > 0$. The open boundary condition implies that all waves must be outgoing waves beyond some surface of last scattering, e.g., a spherical outgoing wave of the form $\exp[-i\tilde{\omega}_n(t - r/c)]/r$, where c is the light speed in free space. The combination of causality and the outgoing boundary condition leads to an exponentially diverging field at infinity $\exp[(\gamma_n/c)\, r]$. Therefore, such QNMs are generally not square-integrable. To overcome this difficulty and construct an orthonomal condition necessary for mode expansion, a variety of regularization schemes have been developed to mediate this divergence.[55−61] In general 3D systems, a perfectly matched layer (PML)-based scheme is usually applied to define the inner product[39,40]

$$\langle \tilde{\boldsymbol{E}}_n | \tilde{\boldsymbol{E}}_m \rangle_{3D-PML} = \int_{\Omega \cup \Omega_{PML}} [\tilde{\boldsymbol{E}}_n \cdot \boldsymbol{\varepsilon} \tilde{\boldsymbol{E}}_m - \tilde{\boldsymbol{H}}_n \cdot \boldsymbol{\mu} \tilde{\boldsymbol{H}}_m] dV \tag{3}$$

where the integration domain $\Omega \cup \Omega_{PML}$ consists of the physical finite domain Ω and the PML domain Ω_{PML} implementing the outgoing boundary condition. The unconjugated multiplication and additional boundary term within Ω_{PML} come from the nondegenerate non-Hermiticity[62] and the openness[40] of this resonator system, respectively. The inner product in eq 3 satisfies the biorthogonality relation $\langle \tilde{\boldsymbol{E}}_n | \tilde{\boldsymbol{E}}_m \rangle = \delta_{n,m}$, where $\delta_{n,m}$ is the Kronecker delta.

With the rigorously defined QNM inner product eq 3, a space-dependent field excitation problem can be decomposed into a few space-independent modal excitation contributions.[63] A resonator subject to a source excitation $\boldsymbol{P}(r, t) = \int \boldsymbol{P}(r, \omega) e^{-i\omega t} d\omega$ within the resonator generates electromagnetic field $[\boldsymbol{E}(\boldsymbol{r}), \boldsymbol{H}(\boldsymbol{r})]$ through

$$\nabla \times \boldsymbol{E}(\boldsymbol{r}, \omega) = i\omega \boldsymbol{\mu}(\boldsymbol{r}) \boldsymbol{H}(\boldsymbol{r}, \omega) \tag{4}$$

$$\nabla \times \boldsymbol{H}(\boldsymbol{r}, \omega) = -i\omega[\boldsymbol{\varepsilon}(\boldsymbol{r}) \boldsymbol{E}(\boldsymbol{r}, \omega) + \varepsilon_0 \boldsymbol{P}(\boldsymbol{r}, \omega)] \tag{5}$$

Here, the polarization $\boldsymbol{P}(\boldsymbol{r})$ has the same unit as electric field $\boldsymbol{E}(\boldsymbol{r})$ to be consistent with the discussions of laser dynamics in subsequent sections.[24] $\boldsymbol{P}(\boldsymbol{r}, \omega)$ could have arbitrary spectrum distribution and the excited electromagnetic field $[\boldsymbol{E}(\boldsymbol{r}, \omega), \boldsymbol{H}(\boldsymbol{r}, \omega)]$ would respond according to eq 4. Expanding the fields $[\boldsymbol{E}(\boldsymbol{r}, \omega), \boldsymbol{H}(\boldsymbol{r}, \omega)]$ onto the normalized QNM basis as $\boldsymbol{E}(\boldsymbol{r}, \omega) = \Sigma_n a_n \tilde{\boldsymbol{E}}_n(\boldsymbol{r}, \omega)$ and $\boldsymbol{H}(\boldsymbol{r}, \omega) = \Sigma_n a_n \tilde{\boldsymbol{H}}_n(\boldsymbol{r}, \omega)$, such space-dependent partial differential equations determine a QNM amplitude as[39,40]

$$a_n(\omega) = -\frac{\omega \int \boldsymbol{P}(\boldsymbol{r}, \omega) \cdot \tilde{\boldsymbol{E}}_n(\boldsymbol{r}, \omega) dV}{\omega - \tilde{\omega}_n} \tag{6}$$

https://doi.org/10.1021/acsphotonics.5c00086
ACS Photonics 2025, 12, 4150−4160

The domain of integration spans over the space where $\boldsymbol{P}(\boldsymbol{r})$ is nonzero, which should be confined inside the resonator structure.[39,56] The Lorentzian frequency dependence in eq 6 manifests typical resonant response to a real frequency excitation.

It is worth noting that the expansion above is rigorous for fields within the resonator structure, given the completeness of the entire set of QNMs.[39,40] However, a finite subset of the complete infinite set is always applied in practice, which inevitably introduces limitations and is only valid under certain restrictions.[56] For this particular problem of atomic emission in laser systems, the contribution of higher-order modes is automatically suppressed via the narrow-band laser excitation, and there is no direct coupling from the effective source $\boldsymbol{P}(\boldsymbol{r})$ to the free-space continuum since the lasing atoms reside within the laser cavity. Therefore, the two limitations are automatically mediated here, leading to a physically sound and mathematically safe field decomposition into a small number of QNMs.[56] Additionally, the excited field $\boldsymbol{E}(\boldsymbol{r}, t)$ of non-monochromatic source $\boldsymbol{P}(\boldsymbol{r}, t) = \int \boldsymbol{P}(\boldsymbol{r}, \omega)e^{-i\omega t}d\omega$ can be obtained by superposing a series of monochromatic response $\boldsymbol{E}(\boldsymbol{r}, \omega)$ directly, due to the linear nature of Fourier transform.[39,64]

3. SINGLE-MODE LASING UNDER QNM EXPANSION USING THE PADÉ APPROXIMANT

In this section, we use the QNM expansion framework to investigate the single-mode lasing solution of the *ab initio* MB equations and show how the Padé approximant can be used to accurately account for spatial hole burning. Specifically, the pump-induced polarization density $P(x)$ is considered as the perturbation and the electric field can be reconstructed by the QNM expansion.

Consider a 1D microcavity edge emitting laser shown in Figure 2a.[65,66] The laser medium is modeled as an ensemble of two-level atoms and the light-matter interaction can be described semiclassically by the MB equations.[27,28] When subject to external pumping, a nonzero population inversion builds up and generates a pump-induced polarization density $P(x)$ in the laser medium, providing gain to the laser cavity. As a result, such pump-induced gain begins to compensate for the intrinsic loss of the cavity resonances as the pumping strength increases, until the loss of one QNM is completely compensated. At this point, the original complex QNM frequency $\tilde{\omega}$ shifts to a purely real lasing frequency, and this critical pumping strength is known as the first lasing threshold D_1^{th}. Beyond this lasing threshold, the electric field saturates the gain, thus modifying the distribution of polarization non-linearly, which, in turn, yields a finite electric field from the active cavity. At equilibrium, single-mode lasing operation turns on with a stationary saturated population inversion distribution, $D(x) = [1 + |\Gamma_\perp(\omega_0)|^2|E_0(x)|^2]^{-1} D_{\text{P}}(x)$, where $\Gamma_\perp(\omega) = \frac{\gamma_\perp}{\omega - \omega_{\text{ab}} + i\gamma_\perp}$ stands for the normalized gain curve and $D_{\text{P}}(x) = D_{\max}\text{Win}(x)$ is the space-dependent pumping strength. Here, $D_{\max}$ represents the effective pumping strength and Win (x) is a normalized window function for the pumping profile, which is zero outside the pumped cavity. Typically, Win (x) is not necessarily flat within the laser medium and can be tailored to be spatially nonuniform to boost the laser power-efficiency.[67] ω_0 and $E_0(x)$ are the real frequency and electric field determined by the nonlinear single-mode lasing equation,

$$\frac{d^2E_0(x)}{dx^2} + \left(\frac{\omega_0}{c}\right)^2 \varepsilon_r(x)E_0(x) = -\left(\frac{\omega_0}{c}\right)^2 \Gamma_\perp(\omega_0)D(x)E_0(x) \tag{7}$$

The intensity-dependent term in $D(x)$ accounts for the system's spatial-hole burning, which is the key to gain saturation and multimode lasing operation.

In such 1D multilayer structure, the QNM inner product has a simple analytic form of

$$\langle \tilde{E}_n|\tilde{E}_m\rangle_{1\text{D}} = \int_{x_1}^{x_2} \varepsilon_r(x)\tilde{E}_n(x)\tilde{E}_m(x)dx + i\frac{\tilde{E}_n(x_1)\tilde{E}_m(x_1) + \tilde{E}_n(x_2)\tilde{E}_m(x_2)}{(\tilde{\omega}_n + \tilde{\omega}_m)/c} \tag{8}$$

where $x_{1,2}$ marks the edge of the resonator in the background medium. Accordingly, the expansion coefficients can be expressed as (see derivation in Supporting Information S1)

$$a_n = \frac{\omega^2 \int_{x_1}^{x_2} \tilde{E}_n(x)P(x)dx}{(\tilde{\omega}_n^2 - \omega^2)\langle \tilde{E}_n|\tilde{E}_n\rangle_{1\text{D}}} \tag{9}$$

Under the QNM expansion framework, the spatial coupling is completely included in the QNM profile $\tilde{E}_m(x)$, leaving only the QNM-amplitudes a_n and frequency ω_0 as unknowns. Ideally, the infinite set of QNMs forms a complete basis for dispersion-free permittivity $\varepsilon_r(x)$, so its result should be equivalent to directly solving eq 7. In practice, off-resonance QNM contributions decay according to a Lorentzian function $(\tilde{\omega}_m^2 - \omega^2)^{-1}$, so only near-resonance QNMs dominate the cavity response. For an excitation near a single resonance $\omega \approx \tilde{\omega}_n$, the single-mode lasing eq eq 7 can be simplified by the QNM expansion eq eq 9 with single QNM contribution $E_0(x) \approx a_n\tilde{E}_n(x)$ as,[28]

$$(\tilde{\omega}_n^2 - \omega_0^2)\langle \tilde{E}_n|\tilde{E}_n\rangle = \omega_0^2\Gamma_\perp(\omega_0)D_{\max}F[|\Gamma_\perp(\omega_0)a_n|^2] \tag{10}$$

where $F(y) = \int_{\text{cav}} \frac{\text{Win}(x)\tilde{E}_n^2(x)}{1+|\tilde{E}_n(x)|^2 y}dx$ is an integral function defined across the cavity.

Equation 10 is a nonlinear integral equation of unknowns $\{a_n, \omega_0\}$. Typical iterative nonlinear methods for solving such an integral equation require multiple evaluations of the original function, which makes the calculation of $F(y)$ a bottleneck of computation. Here, we find that a rational function expansion suffices to provide an accurate estimation of the integral function $F(y)$,

$$F(y) = \int_0^L \frac{\text{Win}(x)E_\alpha(x)^2}{1 + |E_\alpha(x)|^2 y}dx \approx \frac{\lambda}{1 + \mu y} \tag{11}$$

This is referred to as the Padé approximant of order $[0/1]$ for function $F(y)$,[68,69] where the series coefficients $\{\lambda, \mu\}$ can be numerically fitted from some precomputed function values, as shown in Figure 2b and discussed in Supporting Information S5. Therefore, eq 10 for single-mode lasing reduces to a purely algebraic equation under a Padé approximant eq 11. The pump-dependent intensity and mode pattern are plotted in Figure 2c,d for single-mode lasing solutions using the QNM expansion and direct FDFD method without approximation,[29] respectively. By comparing results of the two methods, one can conclude that QNM expansion accurately reproduces the single-mode lasing solution. The residual quantitative error

https://doi.org/10.1021/acsphotonics.5c00086
ACS Photonics 2025, 12, 4150−4160

comes from the neglect of other QNMs' excitations and the use of Padé approximant.

Notably, the nearly linear relationship between the laser intensity and the pumping strength is reflected in both results in Figure 2. This phenomena can be readily derived from conventional interpretation of static saturable gain $g = g_0/(1 + I/I_{sat})$. Stable lasing requires complete gain-loss cancellation $g = l$, thus a linear dependence $g_0 = (1 + I/I_{sat})\ l$ is established between the intensity I and the unsaturated gain g_0, which is proportional to the pumping strength D_{max}, as the loss rate l can be considered constant for a given lasing mode. However, the description of saturable gain sometimes oversimplifies the gain mechanism and cannot directly connect to the *ab initio* description of MB equations, in which saturation appears as a local property known as spatial hole burning and extends the design space for laser cavities.[67] Meanwhile, the linear dependence is also not straightforward from the *ab initio* single-mode lasing eq 7.

By approximating the lasing mode as a single QNM mode, one can unify these two different descriptions and provide a complete expression of the nearly linear relation. Without external pumping, eq 10 reduces to $\omega_0 = \tilde{\omega}_n$, meaning that the electric field decays at the same loss rate $l = -\mathrm{Im}[\tilde{\omega}_n]$ of QNM $\tilde{E}_n(x)$. Operating in the single-mode lasing regime means that the complex frequency change given by eq 10 has to completely cancel the intrinsic loss rate $l = -\mathrm{Im}[\tilde{\omega}_n]$, leading to a real lasing frequency ω_0. As a result, by inserting eq 11 into eq 10, one can obtain a closed-form expression of the relation between laser intensity, frequency, and pumping strength,

$$(\tilde{\omega}_n^2 - \omega_0^2)\langle\tilde{E}_n|\tilde{E}_n\rangle[1 + \mu|\Gamma_\perp(\omega_0)a_n|^2] = \omega_0^2\Gamma_\perp(\omega_0)\lambda D_{max} \tag{12}$$

As pumping strength D_{max} increases, the change in laser frequency is typically negligible so that eq 12 predicts a linear dependence between pumping strength D_{max} and the laser intensity, which is proportional to $|a_n|^2$. Therefore, the QNM expansion combined with the Padé approximant establishes the connection between the static saturable gain and local spatial hole burning. It is important to emphasize that the Padé approximant is not merely a mathematical approximation, it is also rooted in the physics of saturable gain. The typical phenomenological description of saturable gain $g = g_0/(1 + I/I_{sat})$ does not include the spatial dependence, implicitly assuming a uniform distribution of both the laser medium and field intensity. Moreover, such a description of saturable gain can successfully model many laser behaviors even though, in practice, both the pumping strength and the field intensity can be nonuniform within the laser cavity. Here, this conflict of nonuniformity is resolved by the high accuracy of Padé approximant, ensuring the effectiveness of such traditional saturable gain descriptions with the inherent spatially nonuniform laser nonlinearity.

It is worth noting that similar linear-dependence has been found via the so-called single-pole approximation of SALT (SPA-SALT),[28] where a different basis function is used and the lasing frequency is assumed to be fixed. However, tracing the frequency change can be critical when a system is operating near an EP, which justifies the significance of the QNM expansion analysis here.

4. DYNAMIC GAIN AND FREQUENCY COMB GENERATION IN NEAR-EP LASERS UNDER QNM-PALT

Typically, adding pump power to a single-mode laser will result in a second cavity resonance reaching its lasing threshold by taking advantage of the undepleted gain at the locations in the cavity where the first mode does not have much intensity. In this process the population inversion can remain static and yields stable two-mode lasing.[28] However, if the system is operating close to an EP, a second frequency component can, and generally will, be populated with long-lived excitations due to spontaneous emission even when the second cavity resonance is below its lasing threshold.[24] The nonlinear coupling between these two close-but-different frequencies can destabilize the stationary gain and initiate a synchronized oscillation between the population inversion and electric field. The frequency difference determines the oscillation frequency of population inversion, which then acts as a time-modulation to the fields within the gain medium. Thus, additional frequencies emerge through this self-time-modulation process and form a frequency comb with periodic population inversion. Such laser dynamics have been numerically demonstrated using PALT, a frequency domain analysis of the MB equations.[24] Nevertheless, PALT also poses great challenges on both intuitive interpretation and numerical computation of dynamic gain due to the combination of nonlinear couplings across different time scales and spatial complexity. Previously, the only feasible numerical approach for PALT relied on the fact that the response of 1D systems can be analytically described via a Green's function,[24] which requires strict initial guesses and long computation times. Here, we show that PALT can be further simplified via QNM expansion using a Padé approximant to handle these difficulties, yielding an efficient algorithm even when applied to multidimensional systems.

Starting from the PALT analysis, the EP-laser dynamics in 1D system can be described by[24]

$$\frac{d^2E_m(x)}{dx^2} + \frac{\omega_m^2}{c^2}\varepsilon_r(x)E_m(x) = -\frac{\omega_m^2}{c^2}\Gamma_\perp(\omega_m)\sum_{n=-\infty}^{+\infty} D_{m-n}(x)E_n(x) \tag{13}$$

$$\bar{D}(x) = D_p(x)[\bar{\bar{I}} - (1/2)\bar{\bar{\Gamma}}_{\|}(\bar{\bar{E}}(x)^\dagger\bar{\bar{\Gamma}}_+\bar{\bar{E}}(x) - \bar{\bar{E}}(x)\bar{\bar{\Gamma}}_-^\dagger\bar{\bar{E}}(x)^\dagger)]^{-1}\bar{\delta} \tag{14}$$

where $\omega_m = \omega_0 + m\omega_d$ is the frequency of the mth Fourier component $E_m(x)\ e^{-i\omega_m t}$. All of these Fourier components are coupled together through the dynamic population inversion $D(x, t = \sum_n D_n(x)\ e^{-in\omega_d t})$ determined by eq 14, where $\bar{D}(x)$ and $\bar{\delta}$ are column vectors with components $(\bar{D}(x))_m = D_m(x)$ and $(\bar{\delta}_m = \delta_{m,0})$; again, $\delta_{m,0}$ is the Kronecker delta. $\bar{\bar{E}}(x)$ is a matrix formed from the electric fields of each different Fourier component $(\bar{\bar{E}}(x))_{mn} = E_{m-n}(x)$. $\bar{\bar{\Gamma}}_{\|}$ and $\bar{\bar{\Gamma}}_{\pm}$ are diagonal matrices with $(\bar{\bar{\Gamma}}_{\|})_{mn} = \delta_{m-n}\gamma_{\|}/(m\omega_d + i\gamma_{\|})$ and $(\bar{\bar{\Gamma}}_{\pm})_{mn} = \delta_{m-n}\Gamma_\perp(\omega_{\pm m})$, representing the dispersive response of the two-level atoms. $\gamma_{\|}$ is the relaxation rate of population and $\bar{\bar{I}}$ is the identity matrix. Equation 14 describes how a static

https://doi.org/10.1021/acsphotonics.5c00086
ACS Photonics 2025, 12, 4150−4160

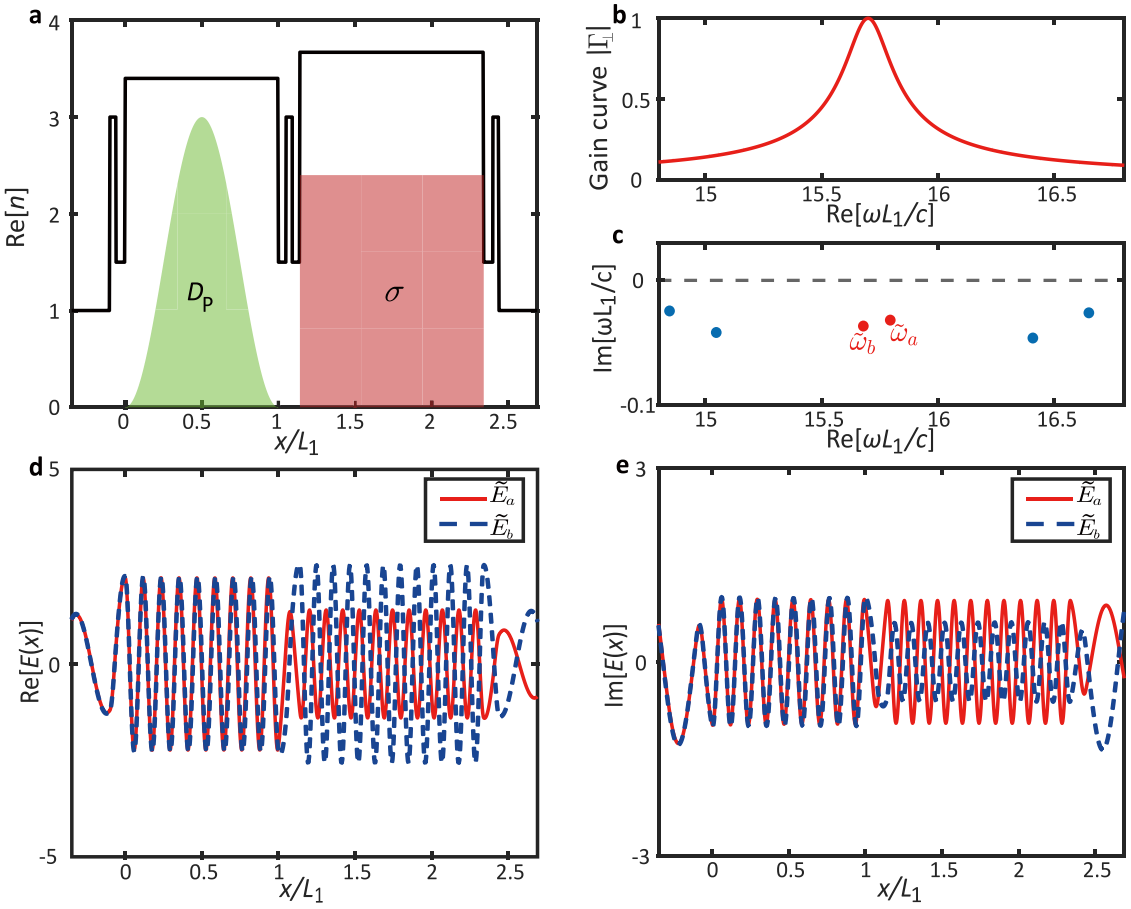

Figure 3. (a) The refractive index profile of the coupled gain-loss resonator. The green area stands for the pump profile and the red area represents the passive conductivity σ. The pump profile is tapered to a Hann window function Win $(x) = 1 - \cos(2\pi x/L_1)$ within the active cavity and the gain parameters are $\gamma_\perp = 0.1\ c/L_1$ and $\gamma_\parallel = 0.002\ c/L_1$. The conductivity σ is tuned when increasing pumping strength to ensure the laser operates near EP. (b) Absolute value of the normalized gain curve $\Gamma_\perp(\omega)$. (c) Distribution of QNM frequencies on the complex frequency plane. The two modes around the center of gain curve have biggest excitation amplitude thus are colored red. (d, e) The real and imaginary part of the QNM field profile $E_{a,b}$ across the resonator. These two modes share similar profile inside the two cavities with a constant phase different.

pump $D_p(x)$ is saturated and modulated locally by the electric field $E(x) = \sum_m E_m(x)\ e^{-i\omega_m t}$, and then the induced polarization density serves as an excitation source to support the stable generation of frequency comb through eq 13.

For illustrative purposes, we consider a parity-time-symmetric-like configuration as shown in Figure 3a, where the pumped cavity is coupled to the passive cavity with linear material loss. The real part of refractive indexes of the pumped and lossy cavities are $n_1 = 3.4$ and $n_2 = 3.67$. The system is normalized by the length of pumped cavity $L_1 = 2.05\ \mu$m, and the length of the lossy cavity is $L_2 = 1.2L_1$. Two DBRs are used at both ends of the structure to control the radiation loss, and its corresponding refractive indexes and lengths are $[n = 3.0, L = 0.04\ L_1]$ and $[n = 1.5, L = 0.06\ L_1]$. The DBR in the middle regulates the coupling between the two cavity modes, and its refractive indexes and lengths are $[n = 3.0, L = 0.04\ L_1]$ and $[n = 1.5, L = 0.05\ L_1]$. The active cavity C_{act} on the left is immersed in a tapered static pump $D_p(x)$ and the passive cavity C_{pas} on the right has linear absorption in terms of a complex permittivity $\varepsilon_r(x) = n_2^2 + i\sigma/\omega$, where σ is the passive conductivity that yields absorption. The pump provides dispersive gain to signals at different frequencies, and the corresponding modulus of normalized gain curve $\Gamma_\perp(\omega) = \frac{\gamma_\perp}{\omega - \omega_{ab} + i\gamma_\perp}$ is shown in Figure 3b. Such a coupled-cavity structure has its QNM frequencies located below the real axis as shown in Figure 3c. The two QNMs around the center of the gain curve receive most gain compared with other QNMs and constitute the EP pair we will focus on through this section. The field profiles of the EP pair are depicted across the coupled-cavity system in Figure 3d,e, which show similar field profiles within each cavity and a cross-cavity tunneling due to the weak spatial coupling suppressed by the DBR in the middle.

Solving the spatial-temporally coupled nonlinear wave equations, eqs 13−14 reveal the frequency comb formation in this near-EP system. Its exact solution is plotted in Figure 4c as a function of D_{max}, with each line representing the intensity $|E_m(x_0)|^2$ of a comb tooth at the left end of the active cavity C_{act}, $x_0 = 0$. The EP comb spectrum at pumping strength of $D_{max} = 0.2$ is plotted in Figure 4e. Only the central two comb teeth with highest intensity can be continuously connected to the two original passive QNMs, while the rest come from wave mixing induced by the dynamic population inversion. However, since the temporal coupling terms in eqs 13−14 include nonlinear matrix inverse which should be evaluated at every spatial pixel, under standard PALT one has to solve a nonlinear dense matrix problem with a massive number of discretized field amplitudes as unknowns. Although the simplicity of a 1D structure allows a semianalytical Green's

https://doi.org/10.1021/acsphotonics.5c00086
ACS Photonics 2025, 12, 4150−4160

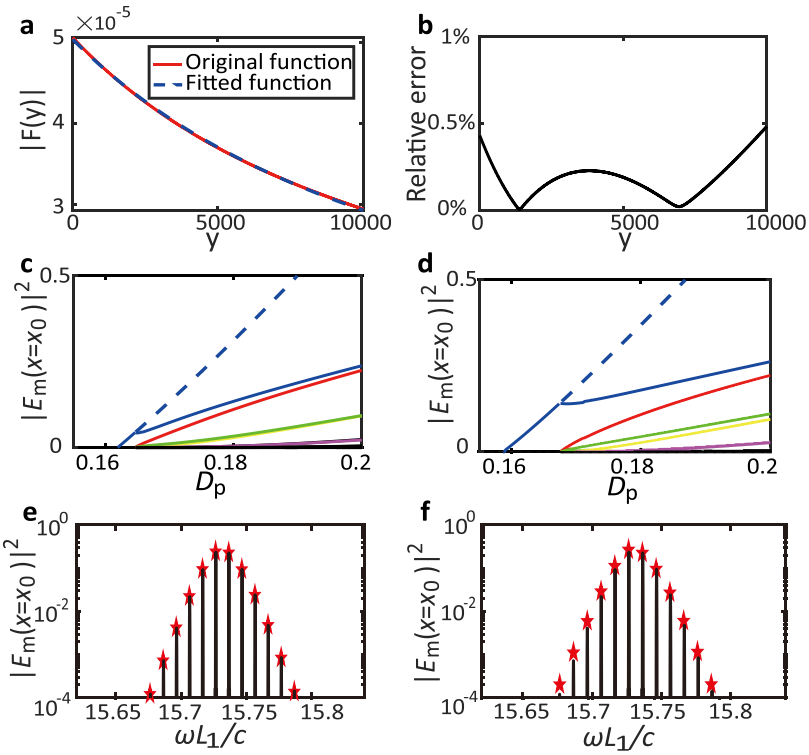

Figure 4. Comparison of computation results from exact Green's function brute-force integration and QNM-PALT. (a) Absolute value of the original integral function $F(y)$ and the fitted function with real variable y. (b) Percentage error of the Padé approximant compared with the exact value. (c, d) Lasing intensities at frequency $\omega_m = \omega_0 + m\omega_d$ as a function of pumping strength D_{max}. The level of absorption σ is tuned with the pump to ensure near-EP operation (see in Supporting Information S3). (e, f) The comb spectrum at pumping strength of $D_{max} = 0.2$ are marked as red pentagrams. The solid black line represents the spectrum calculated from a direct FDTD simulation. (c, e) are the exact result from Green's function and (d, f) are from QNM-PALT under Padé approximant.

function approach for numerical computation,[24] it is generally impractical to implement in more complicated structures in 2D and 3D.

Instead, under the QNM expansion framework, the spatial dependence of PALT equations can be included in the QNM basis, leaving only a few temporally coupled amplitudes as unknowns. Moreover, as the pump-induced polarization in eq 13 is bounded by the bandwidth of the gain curve shown in Figure 3b, the two near-resonance QNM excitations marked as red dots in Figure 3c dominate the passive cavity response. As the pumping strength D_{max} gradually increases from 0, these two complex QNM frequencies can continuously connect to the two central frequencies of the comb spectrum (see in Supporting Information Figure S1), and the frequency-mixing of which generates polarizations at equally spaced frequencies around the original two. Those polarizations then act as additional source to excite electric field on the other comb lines, which could be readily modeled by the QNM expansion approach. Additionally, we notice that these two QNMs shown in Figure 3d,e have almost the same field spatial profile $E_\alpha(x)$ inside the pumped cavity $\tilde{E}_{a,b}(x) = \alpha_{1,2}E_\alpha(x)$, guaranteed by the weak spatial coupling limit in such EP-laser.[24] By projecting the electric field onto the near-resonance 2-QNM basis as $E_m(x) = a_m\tilde{E}_a(x) + b_m\tilde{E}_b(x)$ and adopting the same profile approximation, eq 13 can be simplified as a set of nonlinear matrix integral equations with the QNM amplitudes $\{a_m, b_m\}$ and frequencies $\{\omega_0, \omega_d\}$ as unknowns (see detailed derivation in Supporting Information S4),

$$(\tilde{\omega}_a^2 - \omega_m^2)a_m\langle\tilde{E}_a|\tilde{E}_a\rangle = \omega_m^2 D_{max}\alpha_1\sum_k M_{m-k}(a_k\alpha_1 + b_k\alpha_2) \tag{15}$$

$$(\tilde{\omega}_b^2 - \omega_m^2)b_m\langle\tilde{E}_b|\tilde{E}_b\rangle = \omega_m^2 D_{max}\alpha_2\sum_k M_{m-k}(a_k\alpha_1 + b_k\alpha_2) \tag{16}$$

where M_{m-k} is the coupling coefficient between signals with frequency ω_m and ω_k induced by the $(m-k)$th component D_{m-k} of dynamic population inversion. Inserting the QNM expansion into eq 14, one can determine M_{m-k} by $M_{m-k} = (\bar{M})_{m-k}$, where $\bar{M}$ is a column vector,

$$\bar{M} = \bar{\bar{F}}(\bar{\bar{I}}_{eff})\bar{\delta} \tag{17}$$

Here, $\bar{\bar{F}}(\bar{\bar{I}}_{eff})$ is a matrix generalization of the scalar function $F(y)$ defined as $[\bar{\bar{F}}(\bar{\bar{I}}_{eff})]_{mn} = F[(\bar{\bar{I}}_{eff})_{mn}]$. $\bar{\delta}$ is a column vector with components $(\bar{\delta})_m = \delta_{m,0}$. $\bar{\bar{I}}_{eff}$ is an effective intensity matrix defined as

$$\bar{\bar{I}}_{eff} = \frac{1}{2}\bar{\bar{\Gamma}}_{\|}[(\alpha_1\bar{\bar{a}} + \alpha_2\bar{\bar{b}})\bar{\bar{\Gamma}}_{-}^{\dagger}(\alpha_1^*\bar{\bar{a}}^{\dagger} + \alpha_2^*\bar{\bar{b}}^{\dagger}) - (\alpha_1^*\bar{\bar{a}}^{\dagger} + \alpha_2^*\bar{\bar{b}}^{\dagger})\bar{\bar{\Gamma}}_{+}(\alpha_1\bar{\bar{a}} + \alpha_2\bar{\bar{b}})] \tag{18}$$

where $(\bar{\bar{a}})_{mn} = a_{m-n}$ and $(\bar{\bar{b}})_{mn} = b_{m-n}$ are two amplitude matrices.

Equations 15−18 are the basic QNM-PALT integral equations of the QNM amplitudes $\{a_m, b_m\}$ and frequencies $\{\omega_0, \omega_d\}$. However, elements of $\bar{\bar{I}}_{eff}$ are generally complex and might fall outside the valid domain of Padé approximant,

https://doi.org/10.1021/acsphotonics.5c00086
ACS Photonics 2025, 12, 4150−4160

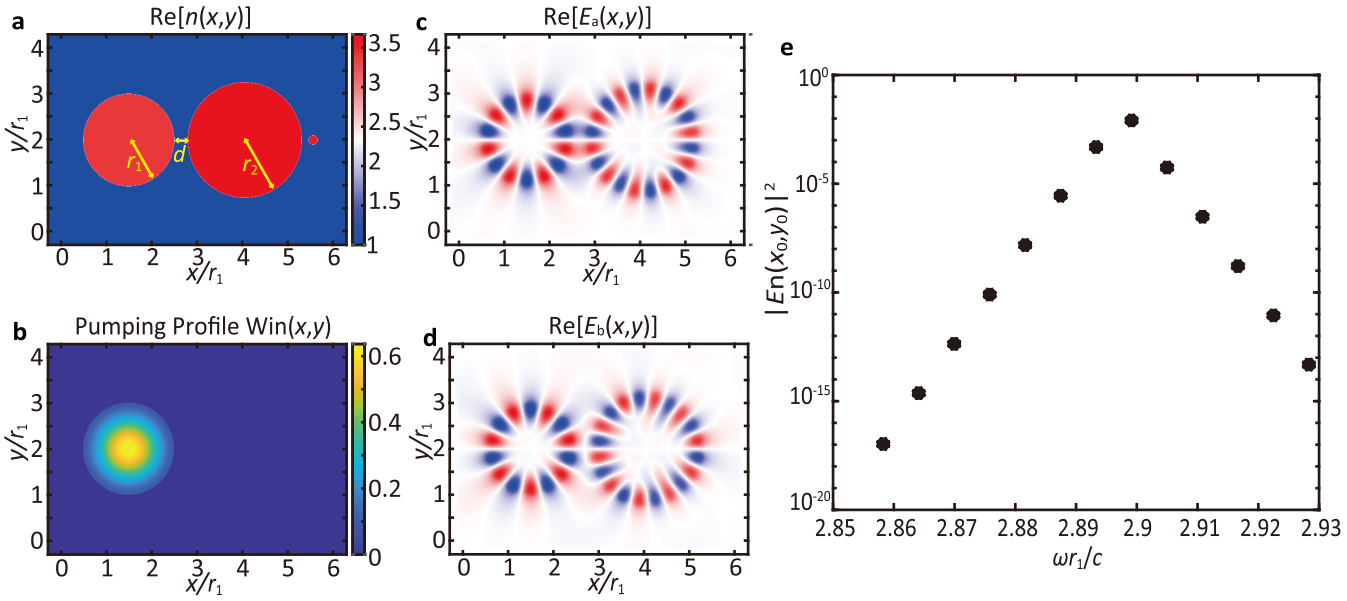

Figure 5. (a) Real part of the refractive index of two coupled disk resonator tuned near an EP. The two disks have different radius $r_2 = 1.25r_1$ and complex refractive index of $n_1 = 3.4 + 0.005i$ and $n_2 = 3.67 + 0.005i$. The distance between two disks is $d = 0.3r_1$. An additional nanotip absorber was placed at a distance of $d_a = 0.15r_1$ from the right disk along the central axis. The nanotip absorber has a radius of $r_a = 0.1r_1$ and a highly lossy refractive index of $n_a = 3.5761 + 0.2525i$. (b) A Gaussian shaped pumping $D = D_{max} \times (2\pi\sigma^2)^{-1}\exp[-r^2/(2\sigma^2)]$, with $\sigma = 0.5r_1$, is applied to the left disk to provide gain to this system. The Gaussian distribution is truncated outside the boundary of the disk and the corresponding gain parameters are $\omega_{ab} = 2.897c/r_1$, $\gamma_\perp = 0.02c/r_1$, and $\gamma_\parallel = 0.004c/r_1$. (c, d) The real part of the field distribution of the two low loss QNMs involved in the lasing action. (e) The comb solution at the pumping strength $D_{max} = 0.8$.

which means Padé approximant cannot be adopted directly to simplify the integral calculation. Noting that $\overline{\overline{I}}_{eff}$ only depends on the QNM amplitudes and has no spatial dependence, its eigenvalues and eigenvectors should also be independent of space. Therefore, its matrix of eigenvectors can be taken out of the integral thus significantly reducing the number of evaluations of $F(y)$ via

$$\bar{M} = \overline{\overline{F}}(\overline{\overline{I}}_{eff})\bar{\delta} = \overline{\overline{F}}(\overline{\overline{P}}^{-1}\overline{\overline{\Lambda}}\overline{\overline{P}})\bar{\delta} = \overline{\overline{P}}^{-1}\overline{\overline{F}}(\overline{\overline{\Lambda}})\overline{\overline{P}}\bar{\delta} \tag{19}$$

where $\overline{\overline{P}}$ and $\overline{\overline{\Lambda}}$ are defined by the diagonalization of $\overline{\overline{I}}_{eff} = \overline{\overline{P}}^{-1}\overline{\overline{\Lambda}}\overline{\overline{P}}$. One only needs to evaluate $F(y)$ at the diagonal elements since $\overline{\overline{\Lambda}}$ is the diagonal eigenvalue matrix. Moreover, as evidenced in Supporting Information S5, all the eigenvalues in $\overline{\overline{\Lambda}}$ reside within the valid domain of Padé approximant, so all the integrals can be further simplified by Padé approximant accurately. As a result, the QNM-PALT equations (eqs 15−18) reduce to purely algebraic nonlinear equations without any spatial dependence or integration.

As illustrated in Figure 4a,b, this Padé approximant provides a rather accurate estimation of $F(y)$ for real y and can be analytically continued to a finite area on the complex y plane (a more detailed discussion about the analytic continuation and its accuracy is provided in Supporting Information S5). Solving these nonlinearly coupled algebraic QNM-PALT equations yields numerical results shown in Figure 4d,f. The corresponding comb spectrum is quantitatively reproduced by our QNM-PALT formalism, as also evidenced by the agreement with a direct FDTD simulation. The residual quantitative error comes from the neglect of other QNMs' excitations and the use of Padé approximant.

The original PALT equations (eqs 13−14) define a matrix problem sparsely coupled in space but densely coupled in frequency. Direct solution approaches such as finite-difference frequency domain (FDFD) are impractical due to the small discretization size required and high density of this matrix problem.[29] Even though FDTD simulation could produce satisfactory results in simple 1D systems,[24] the small discretization length and long relaxation time make the numerical simulation extremely inefficient and impossible to scale up to more realistic 2D or 3D structures. As an example, the FDTD results shown in Figure 4e,f require an extremely high resolution of at least 1000 pixels per in-medium wavelength to converge, leading to an FDTD simulation of around 20000 pixels and 8000000 time steps. Such an FDTD simulation of the MB equations in 1D system takes around 10 h on standard hardware, and the simulation time scales quadratically with the resolution of pixels. (A more detailed discussion of the FDTD efficiency can be found in Supporting Information S6). Although a Green's function can analytically describe spatial dependence in Maxwell equation for 1D systems, the spatially nonuniform population inversion still requires fine spatial discretization and restricts the Green's function approach to simple 1D structures.[24] Typical iterative Green's function solvers require a strict initial guess and take around 10 min (with the same hardware setup) to obtain the result shown in Figure 4e.[24] Instead, the QNM-PALT we develop here completely eliminates the space dependence in PALT and provides an accurate description of the coupling strength among different frequencies. The issue of discretizing nonuniform population inversion is circumvented by reconstruction from the QNM expansion coefficients and the field profile of QNM, so spatial discretization on population inversion is no longer needed in QNM-PALT. As a result, QNM-PALT only takes a few seconds to obtain the result shown in Figure 4f with a random initial guess. Furthermore, the QNM-PALT formalism does not depend on the physical dimension of the system and can therefore be directly

https://doi.org/10.1021/acsphotonics.5c00086
ACS Photonics 2025, 12, 4150−4160

generalized to 2D and 3D structures—one just need to replace the 1D QNM inner product eq 8 with the form of the practical dimension.[39]

5. 2D DEMONSTRATION OF EP COMB GENERATION IN COUPLED-DISK RESONATORS

In this section, we apply the QNM-PALT framework to a more realistic 2D coupled-disk structure, where the whispering-gallery modes (WGMs) supported have been shown to be ideal candidates for EP-related lasing applications.[17,18,20]

Here we consider the TM modes in a near-EP laser system consists of two microdisk resonators as illustrated in Figure 5a. Each of the two microdisk resonators naturally supports two degenerate WGMs because of circular symmetry. For such coupled-disk system, the two pairs of degenerate WGMs coupled together, giving rise to 4 nearly degenerate supermodes with different mirror symmetries. In order to manifest a 2-mode EP, a small nanotip with large absorption is introduced along the central axis, effectively suppressing 2 supermodes far below threshold while keep the low loss of other 2 supermodes. The real part of the field distribution of these two high Q supermodes are plotted in Figure 5c,d. A tapered pumping is applied only to the left microdisk as shown in Figure 5b to create the gain-loss contrast crucial to EP formation. In this 2D system, one can use the QNM-PALT framework to find a EP comb solution at the pumping strength of $D_{\max} = 0.8$ shown in Figure 5e. Here, the 1D QNM-PALT equation (eqs 15−16) should be reformulated for general 2D/3D systems as

$$(\tilde{\omega}_a - \omega_m)a_m = \omega_m D_{\max}\alpha_1 \sum_k M_{m-k}(a_k\alpha_1 + b_k\alpha_2) \tag{20}$$

$$(\tilde{\omega}_b - \omega_m)b_m = \omega_m D_{\max}\alpha_2 \sum_k M_{m-k}(a_k\alpha_1 + b_k\alpha_2) \tag{21}$$

where the QNMs are already normalized and the scalar function $F(y)$ in the coupling coefficient matrix $\bar{M}$ should be replaced with corresponding 2D surface (3D volume) integral, which is estimated by its Padé approximant. The complete trajectory of the two EP modes from passive QNMs to the ultimate comb solution is included in Supporting Information S7.

A 2D MB FDTD simulation would require over 2.5×10^6 discretization pixels and 1200 h to obtain an EP comb solution in system shown in Figure 5 (estimated using the same convergence criteria s in 1D). In contrast, our QNM-PALT framework generates the result in Figure 5e within seconds. The high-resolution discretization is only needed in the linear problem of solving QNMs, which takes just minutes with existing efficient algorithms.[70,71] This dramatic speed-up arises because QNM-PALT completely eliminates spatial dependence, making it scalable to arbitrary dimensions.

6. DISCUSSION

The dynamic distribution of population inversion in near-EP lasers has been fully described by the PALT theory,[24] which predicts the self-generation of a frequency comb near an EP. However, it is still challenging to numerically model the coupling between local laser nonlinearity and resonant modal interaction of EP, especially in 2D and 3D. The QNM-PALT framework we developed here provides a systematic approach to bridge these two processes at different time scales. Unlike traditional phenomenological TCMT, which is constructed empirically and might require numerical experiments to fit key parameters such as coupling coefficients and decaying rates,[22,72,73] QNM-PALT utilizes the rigorously defined QNMs as the basis functions to reconstruct the response of the passive structure to an external laser pump. All key parameters in QNM-PALT have closed-form expressions and can be computed with passive QNM solutions.[39] Compared with existing hybrid laser models combining TCMT and carrier rate equations,[25,31−37] QNM-PALT handles full spatial-temporal dependence in population inversion distribution and minimizes the computational burden. Altogether, by inheriting both the conciseness of TCMT and the rigor of *ab initio* MB equations, QNM-PALT provides a minimal model to describe the dynamic gain in EP-lasers, in which many interesting EP behaviors realized on other nonlinear platforms can hopefully be revisited in the context of laser nonlinearity.[44−46,74−77] Moreover, the spatial degree of freedom in laser design can also be efficiently investigated using our approach.[67]

Under reasonable approximations, the challenging numerical computation of PALT can be further simplified to the set of algebraic equations comprising QNM-PALT and can be solved with minimal effort using ordinary nonlinear system solvers. In particular, the Padé approximant of the expansion integral function provides an accurate numerical approach to eliminate the spatial dependence in both EP-lasers and typical single-mode lasers. Compared with a regular Taylor series expansion,[63] such a rational function expansion is more consistent with the characteristics of gain saturation and is expected to simplify the spatial dependence in more complicated multimode lasers.[37] The computational simplicity QNM-PALT promises makes it possible for generalizing such EP-lasers to 2D and 3D structures commonly used in on-chip devices, where more degrees of freedom are available for fine-tuning toward EP.[13,14,17−20] Moreover, our approach also enables optimization of the laser cavity to produce high-quality coherent frequency combs with a compact device volume.

7. METHODS

The full range of laser behaviors, including typical single-mode lasing and frequency comb generation in near-EP lasers, is reconstructed using a quasinormal mode expansion (see in Supporting Information S1−S4). The computational challenges arising from the nonuniform distribution of population inversion are addressed by employing a rational function expansion, known as the Padé approximant, as discussed in Supporting Information S5.

■ ASSOCIATED CONTENT

Supporting Information

The Supporting Information is available free of charge at https://pubs.acs.org/doi/10.1021/acsphotonics.5c00086.

Theoretical and numerical methods used in this study (PDF)

■ AUTHOR INFORMATION

Corresponding Authors

Hao He − *Ming Hsieh Department of Electrical and Computer Engineering, University of Southern California, Los Angeles, California 90089, United States;* orcid.org/0000-0002-2121-2745; Email: hehao@usc.edu

Alexander Cerjan − *Center for Integrated Nanotechnologies, Sandia National Laboratories, Albuquerque, New Mexico*

https://doi.org/10.1021/acsphotonics.5c00086
ACS Photonics 2025, 12, 4150−4160

87185, United States; orcid.org/0000-0002-4362-7300; Email: awcerja@sandia.gov

Authors

Xingwei Gao − *Ming Hsieh Department of Electrical and Computer Engineering, University of Southern California, Los Angeles, California 90089, United States;* orcid.org/0000-0001-8160-7426

Chia Wei Hsu − *Ming Hsieh Department of Electrical and Computer Engineering, University of Southern California, Los Angeles, California 90089, United States;* orcid.org/0000-0002-9609-7155

Complete contact information is available at: https://pubs.acs.org/10.1021/acsphotonics.5c00086

Notes

The authors declare no competing financial interest.

■ ACKNOWLEDGMENTS

A.C. acknowledges support from the Laboratory Directed Research and Development program at Sandia National Laboratories. This work was performed in part at the Center for Integrated Nanotechnologies, an Office of Science User Facility operated for the U.S. Department of Energy (DOE) Office of Science. Sandia National Laboratories is a multimission laboratory managed and operated by National Technology & Engineering Solutions of Sandia, LLC, a wholly owned subsidiary of Honeywell International, Inc., for the U.S. DOE's National Nuclear Security Administration under Contract No. DE-NA-0003525. The views expressed in the article do not necessarily represent the views of the U.S. DOE or the United States Government.

■ REFERENCES

(1) El-Ganainy, R.; Makris, K. G.; Khajavikhan, M.; Musslimani, Z. H.; Rotter, S.; Christodoulides, D. N. Non-Hermitian physics and PT symmetry. *Nat. Phys.* **2018**, *14*, 11−19.

(2) Miri, M.-A.; Alu, A. Exceptional points in optics and photonics. *Science* **2019**, *363*, No. eaar7709.

(3) Özdemir, Ş. K.; Rotter, S.; Nori, F.; Yang, L. Parity-time symmetry and exceptional points in photonics. *Nat. Mater.* **2019**, *18*, 783−798.

(4) Li, A.; Wei, H.; Cotrufo, M.; Chen, W.; Mann, S.; Ni, X.; Xu, B.; Chen, J.; Wang, J.; Fan, S.; et al. Exceptional points and non-Hermitian photonics at the nanoscale. *Nat. Nanotechnol.* **2023**, *18*, 706−720.

(5) Hodaei, H.; Hassan, A. U.; Wittek, S.; Garcia-Gracia, H.; El-Ganainy, R.; Christodoulides, D. N.; Khajavikhan, M. Enhanced sensitivity at higher-order exceptional points. *Nature* **2017**, *548*, 187−191.

(6) Hokmabadi, M. P.; Schumer, A.; Christodoulides, D. N.; Khajavikhan, M. Non-Hermitian ring laser gyroscopes with enhanced Sagnac sensitivity. *Nature* **2019**, *576*, 70−74.

(7) Lai, Y.-H.; Lu, Y.-K.; Suh, M.-G.; Yuan, Z.; Vahala, K. Observation of the exceptional-point-enhanced Sagnac effect. *Nature* **2019**, *576*, 65−69.

(8) Wiersig, J.; Kim, S. W.; Hentschel, M. Asymmetric scattering and nonorthogonal mode patterns in optical microspirals. *Phys. Rev. A:At., Mol., Opt. Phys.* **2008**, *78*, No. 053809.

(9) Wiersig, J.; Eberspächer, A.; Shim, J.-B.; Ryu, J.-W.; Shinohara, S.; Hentschel, M.; Schomerus, H. Nonorthogonal pairs of copropagating optical modes in deformed microdisk cavities. *Phys. Rev. A:At., Mol., Opt. Phys.* **2011**, *84*, No. 023845.

(10) Peng, B.; Özdemir, Ş. K.; Liertzer, M.; Chen, W.; Kramer, J.; Yılmaz, H.; Wiersig, J.; Rotter, S.; Yang, L. Chiral modes and directional lasing at exceptional points. *Proc. Natl. Acad. Sci. U.S.A.* **2016**, *113*, 6845−6850.

(11) Zhang, Z.; Qiao, X.; Midya, B.; Liu, K.; Sun, J.; Wu, T.; Liu, W.; Agarwal, R.; Jornet, J. M.; Longhi, S.; et al. Tunable topological charge vortex microlaser. *Science* **2020**, *368*, 760−763.

(12) Zhao, H.; Feng, L. Parity-time symmetric photonics. *Natl. Sci. Rev.* **2018**, *5*, 183−199.

(13) Rüter, C. E.; Makris, K. G.; El-Ganainy, R.; Christodoulides, D. N.; Segev, M.; Kip, D. Observation of parity-time symmetry in optics. *Nat. Phys.* **2010**, *6*, 192−195.

(14) Peng, B.; Özdemir, Ş. K.; Lei, F.; Monifi, F.; Gianfreda, M.; Long, G. L.; Fan, S.; Nori, F.; Bender, C. M.; Yang, L. Parity-time-symmetric whispering-gallery microcavities. *Nat. Phys.* **2014**, *10*, 394−398.

(15) Liertzer, M.; Ge, L.; Cerjan, A.; Stone, A. D.; Türeci, H. E.; Rotter, S. Pump-induced exceptional points in lasers. *Phys. Rev. Lett.* **2012**, *108*, No. 173901.

(16) Cerjan, A.; Fan, S. Eigenvalue dynamics in the presence of nonuniform gain and loss. *Phys. Rev. A* **2016**, *94*, No. 033857.

(17) Peng, B.; Özdemir, Ş.; Rotter, S.; Yilmaz, H.; Liertzer, M.; Monifi, F.; Bender, C.; Nori, F.; Yang, L. Loss-induced suppression and revival of lasing. *Science* **2014**, *346*, 328−332.

(18) Brandstetter, M.; Liertzer, M.; Deutsch, C.; Klang, P.; Schöberl, J.; Türeci, H. E.; Strasser, G.; Unterrainer, K.; Rotter, S. Reversing the pump dependence of a laser at an exceptional point. *Nat. Commun.* **2014**, *5*, No. 4034.

(19) Feng, L.; Wong, Z. J.; Ma, R.-M.; Wang, Y.; Zhang, X. Single-mode laser by parity-time symmetry breaking. *Science* **2014**, *346*, 972−975.

(20) Hodaei, H.; Miri, M.-A.; Heinrich, M.; Christodoulides, D. N.; Khajavikhan, M. Parity-time-symmetric microring lasers. *Science* **2014**, *346*, 975−978.

(21) Zhang, J.; Peng, B.; Özdemir, Ş. K.; Pichler, K.; Krimer, D. O.; Zhao, G.; Nori, F.; Liu, Y.-x.; Rotter, S.; Yang, L. A phonon laser operating at an exceptional point. *Nat. Photonics* **2018**, *12*, 479−484.

(22) Wang, H.; Lai, Y.-H.; Yuan, Z.; Suh, M.-G.; Vahala, K. Petermann-factor sensitivity limit near an exceptional point in a Brillouin ring laser gyroscope. *Nat. Commun.* **2020**, *11*, No. 1610.

(23) Benzaouia, M.; Stone, A. D.; Johnson, S. G. Nonlinear exceptional-point lasing with ab initio Maxwell−Bloch theory. *APL Photonics* **2022**, *7*, No. 121303.

(24) Gao, X.; He, H.; Sobolewski, S.; Cerjan, A.; Hsu, C. W. Dynamic gain and frequency comb formation in exceptional-point lasers. *Nat. Commun.* **2024**, *15*, No. 8618.

(25) Ji, K.; Zhong, Q.; Ge, L.; Beaudoin, G.; Sagnes, I.; Raineri, F.; El-Ganainy, R.; Yacomotti, A. M. Tracking exceptional points above the lasing threshold. *Nat. Commun.* **2023**, *14*, No. 8304.

(26) Drong, M.; Peřina, J., Jr; Fördös, T.; Jaffrès, H. Y.; Postava, K.; Drouhin, H.-J. Spin vertical-cavity surface-emitting lasers with linear gain anisotropy: Prediction of exceptional points and nontrivial dynamical regimes. *Phys. Rev. A* **2023**, *107*, No. 033509.

(27) Türeci, H. E.; Stone, A. D.; Collier, B. Self-consistent multimode lasing theory for complex or random lasing media. *Phys. Rev. A:At., Mol., Opt. Phys.* **2006**, *74*, 043822.

(28) Ge, L.; Chong, Y. D.; Stone, A. D. Steady-state ab initio laser theory: generalizations and analytic results. *Phys. Rev. A* **2010**, *82*, No. 063824.

(29) Esterhazy, S.; Liu, D.; Liertzer, M.; Cerjan, A.; Ge, L.; Makris, K.; Stone, A. D.; Melenk, J. M.; Johnson, S. G.; Rotter, S. Scalable numerical approach for the steady-state ab initio laser theory. *Phys. Rev. A* **2014**, *90*, No. 023816.

(30) Ge, L.; Tandy, R. J.; Stone, A. D.; Türeci, H. E. Quantitative verification of ab initio self-consistent laser theory. *Opt. Express* **2008**, *16*, 16895−16902.

(31) Chua, S.-L.; Caccamise, C. A.; Phillips, D. J.; Joannopoulos, J. D.; Soljačić, M.; Everitt, H. O.; Bravo-Abad, J. Spatio-temporal theory of lasing action in optically-pumped rotationally excited molecular gases. *Opt. Express* **2011**, *19*, 7513−7529.

(32) Nousios, G.; Christopoulos, T.; Tsilipakos, O.; Kriezis, E. E. Integrated lasers with transition-metal-dichalcogenide heterostructures: Analysis and design utilizing coupled-mode theory for two-dimensional materials. *Phys. Rev. Appl.* **2023**, *19*, No. 064027.
(33) Rasmussen, T. S.; Yu, Y.; Mork, J. Theory of Self-pulsing in photonic crystal fano lasers. *Laser Photonics Rev.* **2017**, *11*, No. 1700089.
(34) Yu, Y.; Xue, W.; Semenova, E.; Yvind, K.; Mork, J. Demonstration of a self-pulsing photonic crystal Fano laser. *Nat. Photonics* **2017**, *11*, 81−84.
(35) Mork, J.; Chen, Y.; Heuck, M. Photonic crystal Fano laser: terahertz modulation and ultrashort pulse generation. *Phys. Rev. Lett.* **2014**, *113*, No. 163901.
(36) Ataloglou, V. G.; Christopoulos, T.; Kriezis, E. E. Nonlinear coupled-mode-theory framework for graphene-induced saturable absorption in nanophotonic resonant structures. *Phys. Rev. A* **2018**, *97*, No. 063836.
(37) Christopoulos, T.; Tsilipakos, O.; Kriezis, E. E. Temporal coupled-mode theory in nonlinear resonant photonics: From basic principles to contemporary systems with 2D materials, dispersion, loss, and gain. *J. Appl. Phys.* **2024**, *136*, No. 011101.
(38) Siegman, A. E. *Lasers*; University Science Books, 1986.
(39) Lalanne, P.; Yan, W.; Vynck, K.; Sauvan, C.; Hugonin, J.-P. Light interaction with photonic and plasmonic resonances. *Laser Photonics Rev.* **2018**, *12*, No. 1700113.
(40) Sauvan, C.; Wu, T.; Zarouf, R.; Muljarov, E. A.; Lalanne, P. Normalization, orthogonality, and completeness of quasinormal modes of open systems: the case of electromagnetism. *Opt. Express* **2022**, *30*, 6846−6885.
(41) Zhang, H.; Miller, O. D. Quasinormal Coupled Mode Theory. 2020 https://arxiv.org/abs/2010.08650.
(42) Binkowski, F.; Betz, F.; Colom, R.; Hammerschmidt, M.; Zschiedrich, L.; Burger, S. Quasinormal mode expansion of optical far-field quantities. *Phys. Rev. B* **2020**, *102*, No. 035432.
(43) Alpeggiani, F.; Parappurath, N.; Verhagen, E.; Kuipers, L. Quasinormal-mode expansion of the scattering matrix. *Phys. Rev. X* **2017**, *7*, No. 021035.
(44) Assawaworrarit, S.; Yu, X.; Fan, S. Robust wireless power transfer using a nonlinear parity−time-symmetric circuit. *Nature* **2017**, *546*, 387−390.
(45) Bai, K.; Fang, L.; Liu, T.-R.; Li, J.-Z.; Wan, D.; Xiao, M. Nonlinearity-enabled higher-order exceptional singularities with ultra-enhanced signal-to-noise ratio. *Natl. Sci. Rev.* **2023**, *10*, No. nwac259.
(46) Bai, K.; Liu, T.-R.; Fang, L.; Li, J.-Z.; Lin, C.; Wan, D.; Xiao, M. Observation of Nonlinear Exceptional Points with a Complete Basis in Dynamics. *Phys. Rev. Lett.* **2024**, *132*, No. 073802.
(47) Fang, K.; Yu, Z.; Fan, S. Realizing effective magnetic field for photons by controlling the phase of dynamic modulation. *Nat. Photonics* **2012**, *6*, 782−787.
(48) Galiffi, E.; Tirole, R.; Yin, S.; Li, H.; Vezzoli, S.; Huidobro, P. A.; Silveirinha, M. G.; Sapienza, R.; Alù, A.; Pendry, J. B. Photonics of time-varying media. *Adv. Photonics* **2022**, *4*, No. 014002.
(49) Sounas, D. L.; Alù, A. Non-reciprocal photonics based on time modulation. *Nat. Photonics* **2017**, *11*, 774−783.
(50) Yuan, L.; Lin, Q.; Xiao, M.; Fan, S. Synthetic dimension in photonics. *Optica* **2018**, *5*, 1396−1405.
(51) Gao, X.; He, H.; Chow, W. W.; Cerjan, A.; Hsu, C. W. Bi-stability and period-doubling cascade of frequency combs in exceptional-point lasers. *Nanophotonics* **2025**, *14*, 2259−2266.
(52) Leung, P. T.; Liu, S.; Young, K. Completeness and orthogonality of quasinormal modes in leaky optical cavities. *Phys. Rev. A* **1994**, *49*, No. 3057.
(53) Lee, S.-Y. Decaying and growing eigenmodes in open quantum systems: Biorthogonality and the Petermann factor. *Phys. Rev. A:At., Mol., Opt. Phys.* **2009**, *80*, No. 042104.
(54) Jackson, J. D. *Classical Electrodynamics*; Wiley, 1998.
(55) Ren, J.; Franke, S.; Hughes, S. Quasinormal modes, local density of states, and classical purcell factors for coupled loss-gain resonators. *Phys. Rev. X* **2021**, *11*, No. 041020.
(56) Sauvan, C.; Hugonin, J.-P.; Maksymov, I. S.; Lalanne, P. Theory of the spontaneous optical emission of nanosize photonic and plasmon resonators. *Phys. Rev. Lett.* **2013**, *110*, No. 237401.
(57) Muljarov, E. A.; Langbein, W.; Zimmermann, R. Brillouin-Wigner perturbation theory in open electromagnetic systems. *Europhys. Lett.* **2010**, *92*, No. 50010.
(58) Muljarov, E. A.; Langbein, W. Exact mode volume and Purcell factor of open optical systems. *Phys. Rev. B* **2016**, *94*, No. 235438.
(59) Kristensen, P. T.; Ge, R.-C.; Hughes, S. Normalization of quasinormal modes in leaky optical cavities and plasmonic resonators. *Phys. Rev. A* **2015**, *92*, No. 053810.
(60) Ge, R.-C.; Hughes, S. Design of an efficient single photon source from a metallic nanorod dimer: a quasi-normal mode finite-difference time-domain approach. *Opt. Lett.* **2014**, *39*, 4235−4238.
(61) Zschiedrich, L.; Binkowski, F.; Nikolay, N.; Benson, O.; Kewes, G.; Burger, S. Riesz-projection-based theory of light-matter interaction in dispersive nanoresonators. *Phys. Rev. A* **2018**, *98*, No. 043806.
(62) Sternheim, M. M.; Walker, J. F. Non-Hermitian Hamiltonians, decaying states, and perturbation theory. *Physical Review C* **1972**, *6*, 114.
(63) Gigli, C.; Wu, T.; Marino, G.; Borne, A.; Leo, G.; Lalanne, P. Quasinormal-mode non-hermitian modeling and design in nonlinear nano-optics. *ACS Photonics* **2020**, *7*, 1197−1205.
(64) Faggiani, R.; Losquin, A.; Yang, J.; Marsell, E.; Mikkelsen, A.; Lalanne, P. Modal analysis of the ultrafast dynamics of optical nanoresonators. *ACS Photonics* **2017**, *4*, 897−904.
(65) Cerjan, A.; Chong, Y.; Ge, L.; Stone, A. D. Steady-state ab initio laser theory for n-level lasers. *Opt. Express* **2012**, *20*, 474−488.
(66) Cerjan, A.; Oskooi, A.; Chua, S.-L.; Johnson, S. G. Modeling lasers and saturable absorbers via multilevel atomic media in the Meep FDTD software: Theory and implementation. 2020 https://arxiv.org/abs/2007.09329.
(67) Ge, L.; Malik, O.; Türeci, H. E. Enhancement of laser power-efficiency by control of spatial hole burning interactions. *Nat. Photonics* **2014**, *8*, 871−875.
(68) Baker, G. A., Jr; Gammel, J. L. The Padé Approximant. *J. Math. Anal. Appl.* **1961**, *2*, 21−30.
(69) Baker, G. A., Jr *The Theory and Application of the Padé Approximant Method*; Academic Press, 1964.
(70) Lin, H.-C.; Wang, Z.; Hsu, C. W. Fast multi-source nanophotonic simulations using augmented partial factorization. *Nat. Comput. Sci.* **2022**, *2*, 815−822.
(71) Bai, Q.; Perrin, M.; Sauvan, C.; Hugonin, J.-P.; Lalanne, P. Efficient and intuitive method for the analysis of light scattering by a resonant nanostructure. *Opt. Express* **2013**, *21*, 27371−27382.
(72) Rodriguez, A.; Soljačić, M.; Joannopoulos, J. D.; Johnson, S. G. χ (2) and χ (3) harmonic generation at a critical power in inhomogeneous doubly resonant cavities. *Opt. Express* **2007**, *15*, 7303−7318.
(73) Burgess, I. B.; Rodriguez, A. W.; McCutcheon, M. W.; Bravo-Abad, J.; Zhang, Y.; Johnson, S. G.; Lončar, M. Difference-frequency generation with quantum-limited efficiency in triply-resonant nonlinear cavities. *Opt. Express* **2009**, *17*, 9241−9251.
(74) Wang, H.; Assawaworrarit, S.; Fan, S. Dynamics for encircling an exceptional point in a nonlinear non-Hermitian system. *Opt. Lett.* **2019**, *44*, 638−641.
(75) Bai, K.; Li, J.-Z.; Liu, T.-R.; Fang, L.; Wan, D.; Xiao, M. Nonlinear Exceptional Points with a Complete Basis in Dynamics. *Phys. Rev. Lett.* **2023**, *130*, No. 266901.
(76) Ramezanpour, S.; Bogdanov, A. Tuning exceptional points with Kerr nonlinearity. *Phys. Rev. A* **2021**, *103*, No. 043510.
(77) Pick, A.; Lin, Z.; Jin, W.; Rodriguez, A. W. Enhanced nonlinear frequency conversion and Purcell enhancement at exceptional points. *Phys. Rev. B* **2017**, *96*, No. 224303.

https://doi.org/10.1021/acsphotonics.5c00086
ACS Photonics 2025, 12, 4150−4160